Fast, low-noise, mode-by-mode, cavity-enhanced absorption spectroscopy by diode-laser self-locking

J Morville, S Kassi, M Chenevier, D Romanini

Applied Physics B manuscript No.
(will be inserted by the editor)

Fast, low–noise, mode–by–mode, cavity–enhanced absorption spectroscopy by diode–laser self–locking.

J. Morville[a], S. Kassi[b], M. Chenevier[b] and D. Romanini[b]

[a] Laboratoire de Spectrométrie Ionique et Moléculaire–CNRS UMR 5579,
Université Claude Bernard–Lyon I, Bat. 205
69622 Villeurbanne Cedex, France
[b] Laboratoire de Spectrométrie Physique–CNRS UMR 5588,
Université J. Fourier–Grenoble I,
B.P. 87–38402 Saint Martin d'Hères Cedex, France

Fax: (33)4 72 44 58 71
Mail: jerome.morville@lasim.univ-lyon1.fr

Received: date / Revised version: date

Abstract A new technique of cavity enhanced absorption spectroscopy is described. Molecular absorption spectra are obtained by recording the transmission maxima of the successive TEM_{00} resonances of a high–finesse optical cavity when a Distributed Feed–Back Diode Laser is tuned across them. A noisy cavity output is usually observed in such a measurement since the resonances are spectrally narrower than the laser. We show that a folded (V–shaped) cavity can be used to obtain selective optical feedback from the intracavity field which builds-up at resonance. This induces laser linewidth reduction and frequency locking. The linewidth narrowing eliminates the noisy cavity output, and allows measuring the maximum mode transmissions accurately. The frequency locking makes the laser to scan stepwise through the successive cavity modes. Frequency tuning is thus tightly optimized for cavity mode injection. Our setup for this technique of Optical–Feedback Cavity–Enhanced Absorption Spectroscopy (OF-CEAS) includes a 50 cm folded cavity with finesse ∼20 000 (ringdown time ∼20 μs) and allows recording spectra of up to 200 cavity modes (2 cm^{-1}) using 100 ms laser scans. We obtain a noise equivalent absorption coefficient of $\sim 5\times10^{-10}$/cm for 1 s averaging over scans, with a dynamic range of 4 orders of magnitude.

Key words: cavity enhanced absorption spectroscopy, high–finesse cavities, optical feedback, diode laser self–locking

PACS:
07.88.+y Instruments for environmental pollution measurements
42.55.Px Semiconductor lasers; laser diodes
42.62.Fi Laser spectroscopy

Introduction

In 1962, it was predicted that cavity resonance could be channelled for the enhancement of the optical path length in absorption spectroscopy [1]. Since the development of low loss dielectric super–mirrors [2], high finesse optical cavities have attracted a growing interest in the field of high–sensitivity gas phase spectroscopy. Initially conceived for use with pulsed lasers, Cavity Ring Down Spectroscopy (CRDS) [3,4] was later adapted to continuous wave lasers (CW–CRDS) [5] which allowed higher spectral resolution and higher sensitivity [6]. Several other experimental schemes were also developed to optimize cavity injection with a CW laser, revealing the interest in this idea [7–10,13–15]

Because of the potential applications in environmental, urban, or industrial site monitoring, medical diagnostics, agronomy, *et cetera*, compact CW sources, such as Distributed Feedback Diode Lasers (DFB–DL) [16], External Cavity Diode Lasers (ECDL) [17] and Quantum Cascade Lasers (QCL) [18], have been especially investigated. The performance of CW-CRDS depends on the ability to measure the decay time, or ringdown time, of the optical cavity with high accuracy and high repetition rate, while tuning the laser frequency in a controlled way. The state of the art is to attain absorption detection limits between 10^{-11} and $10^{-12}/cm/\sqrt{Hz}$ [8], but values around $10^{-9}/cm/\sqrt{Hz}$ are more typical. Several laboratory applications of CW-CRDS in trace detection have been recently demonstrated and field measurements are actively under development even exploiting commercially available instruments.

Cavity Enhanced Absorption Spectroscopy (CEAS) is a promising alternative to CW-CRDS. In CEAS, the light intensity continuously transmitted by cavity resonances is recorded, rather than its decay. A simple derivation starting from the Airy formula for the transmission profile of a resonance, shows that the fractional peak intensity reduction $\Delta I/I$ due to a small absorption per pass $\alpha(\nu)L_{\rm cav} \ll 1$, will be given by this absorption multiplied by $2\mathcal{F}/\pi$, where $L_{\rm cav}$ is the cavity length and $\mathcal{F}$ is the cavity finesse. The finesse is defined as the cavity Free Spectral Range (FSR) divided by the FWHM (Full Width at Half Maximum) of the resonances [1]. The finesse thus corresponds to the path length enhancement induced by the cavity. As in CW–CRDS, the major difficulty in CEAS lies in the injection of the laser light into the narrow transmission width of cavity modes. In addition, the stability of the transmission signal depends on the laser source, contrary to CRDS where the cavity decay signal is, in principle, insensitive to source noise. Indeed, the cavity transmission at the passage through a resonance is often affected by a large noise level, determined by the frequency filtering action of the cavity which converts source frequency fluctuations to amplitude fluctuations [19].

Different CEAS approaches have been proposed and can be classified in two categories. The first approach relies upon electronic locking of the laser frequency to a cavity resonance. One of the best electronic locking techniques is the Pound–Drever–Hall scheme [20], in which closely spaced frequency sidebands are added to the laser radiation to give a derivative–like error signal of a cavity resonance when monitoring the light reflected from the cavity. A detection limit as low as $6.4\times10^{-13}/\mathrm{cm}/\sqrt{\mathrm{Hz}}$ with an empty–cavity ringdown time of $50\,\mu$s, was demonstrated [10]. Moreover, the locked laser spectral purity is given by the cavity mode width, placing the spectral resolution of this technique in the kHz range. Heterodyne and cavity enhanced detection were integrated in a technique referred to as NICE–OHMS, which benefits from a noise cancellation property resulting from the constant spacing of cavity modes. This approach delivered a record sensitivity of $10^{-14}/\mathrm{cm}/\sqrt{\mathrm{Hz}}$ [10] in the measurement of sub-Doppler saturation line–dips. Unfortunately, this scheme appears to be rather complex especially when it comes to tuning large spectral regions as needed in applications of molecular spectroscopy. This also exposes the measurement to excess baseline noise due to etaloning structures which typically arise when tuning spectral regions more than 100 MHz wide [11,12]. In other applications (e.g. *in situ* trace gas detection) another practical problem is the sensitivity of an all-electronic frequency locking scheme to mechanical vibrations.

The second approach consists of quickly sweeping the laser frequency through successive cavity modes while monitoring the cavity transmission signal with a relatively slow photodetector. The integrated transmission of each cavity mode is then measured, rather than the peak transmission value, so this technique is often referred to as Integrated Cavity Output Spectroscopy (ICOS) [21]. Such averaging clearly reduces the amplitude noise associated with the laser frequency noise, but integrating the mode profile, rather than looking at its peak, leads to an equivalent absorption pathlength 2 times smaller than the previous case. More important, two additional noise sources affect this technique. The first is the non uniform excitation of the transverse cavity modes which gives the transmitted cavity spectrum a structured noise periodic with the cavity FSR. The second is mirror inhomogeneity and diffraction losses, which change the effective finesse of different transverse modes. This also alters in a periodic manner the cavity enhancement factor. In order to reduce the effect of the discrete cavity mode structure, it is possible to use a cavity geometry far from confocal (giving a highly non–degenerate transverse mode structure) and an injection far from mode–matched. A quasi–continuum of transverse modes is thus excited as the laser scans, and several scans are averaged while the cavity length is modulated to destroy the residual structure [22]. To our knowledge, the interesting alternative solution of using mode matching to inject principally the TEM_{00} modes for CEAS, has never been reported.

A more refined solution to this second approach is to choose a geometry where modes are degenerate in groups which uniformly divide in $N(\gg 1)$ parts the cavity FSR [23,24]. This allows an off-axis incident beam to fold along a complex trajectory which closes onto itself after N cavity round–trips [25]. Then, as the laser passes through resonance with successive groups of degenerate modes, it can be shown that injection results always in the same trajectory, with the same coupled intensity. Because the trajectory is fixed, the mirror surface losses are also the same, and a uniform cavity output is obtained. In contrast to the non–degenerate case, less averaging and no cavity length modulation are needed to attain a good signal-to-noise ratio.

The bandpass–normalized detection limit for the non degenerate case is typically close to the $2\times10^{-8}/\mathrm{cm}/\sqrt{\mathrm{Hz}}$ obtained [22] for a cavity with ringdown times around $7\,\mu$s, while $3\times10^{-11}/\mathrm{cm}/\sqrt{\mathrm{Hz}}$ is a best value reported using the degenerate configuration [23] for a cavity with a ringdown time of $22\,\mu$s.

The primary advantage of the swept–CEAS approach is simplicity. Need for an optical switch and threshold circuit as in CW-CRDS is eliminated, and mode matching is not used. In the case of the degenerate configuration, the need for careful cavity length adjustment and relatively large mirrors (2 inch mirrors were used for the best reported performance [23]) is compensated by better performance and elimination of the optical isolator. One remaining limiting factor is the low level of cavity transmitted signal.

We present here in detail a CEAS approach [26] developed for fast and accurate trace gas measurement, which allows obtaining the value of the peak transmission of TEM_{00} cavity modes during a single laser sweep. This scheme overcomes the low signal level of previous ICOS systems, and completely disposes of intensity fluctuations and noise associated to the laser linewidth. It is based on a Distributed FeedBack Diode Laser (DFB–DL) self–frequency–locked by Optical Feedback (OF) from the resonating intracavity field. We will see that OF locking, much more simple and robust than active electronic frequency locking, gives slow adiabatic passages through the cavity resonances even when fast laser frequency sweeps are applied. The simultaneous laser linewidth narrowing permits recording the maxima of transmission peaks as if the cavity were excited by a perfectly monochromatic source jumping from a resonance directly to the next. Transverse mode matching to the TEM_{00} modes comes essentially for free, and the successive injection of all TEM_{00} modes yields a mode–by–mode spectrum whose data points are highly defined in frequency and uniformly spaced. This last aspect, already exploited by using a stabilized cavity length in cavity ring down spectroscopy [14], is crucial for high precision measurements.

Coupling of DLs to cavities by OF has been extensively used in atomic physics to stabilize and narrow–down DL emission [27–37] or to attain high intracavity fields [38], and it was already recognized that OF locking can be generalized as a tool to provide cavity enhancement of light–matter interactions. Two examples are the measurement of residual cavity mirror birefringence [39] (where we also used OF frequency locking) and the development of an OF–CRDS setup for trace detection [13].

Part of the novelty of the present work resides in the use of a 3 mirrors cavity in place of a confocal 2 mirrors resonator, in order to obtain OF from a V–shaped light trajectory inside the cavity. In a confocal resonator ($N = 2$), the degeneracy of transverse modes allows the existence of a V-trajectory as a superposition of such modes at the resonance frequency. In a V-shaped cavity, this trajectory is obtained as a pure TEM_{00} mode. One major advantage is the possibility of using cavities of arbitrarily high finesse as needed to increase the sensitivity of physical measurements. In a confocal resonator, it is rather well known that the tolerance required on the mirror surface curvature becomes prohibitive as the finesse increases. As cavity modes become narrower, it simply becomes more difficult to have high transverse order modes to become degenerate. In a V–shaped cavity only the fundamental mode is needed and it is not even required to adjust the mirror distance to the confocal position. Another practical advantage, is the possibility of using mirrors of small diameter for setting up a cavity with large base length (50 cm) and an extremely small intracavity sample volume ($\sim 15\,cm^3$).

The paper is composed as follows. We first outline general experimental details common to all the experimental data presented. We then give a description of the DL–cavity coupled system, based on previous theoretical work and our experimental observations, and introduce the fundamental features of cavity injection by OF. From an application–oriented point of view, we discuss the dependence of injection efficiency on the OF phase and amplitude, and on the laser tuning speed. Afterwards, we discuss how optimal experimental conditions may be set for CEAS. We finally present results in gas phase spectroscopy, and illustrate the potential of our technique for real time trace gas monitoring.

1 Experimental.

In the experimental setup of Fig.1, a V-shaped cavity is used as it is perhaps the simplest configuration producing frequency selected OF when the laser frequency enters in resonance with one of the cavity modes. We will see that even an approximate mode matching guarantees that OF–locking to TEM_{00} cavity modes is dominant and eliminates, by competition, the locking and injection of other transverse modes. This will justify considering only TEM_{00} excitation below. All experimental signals and other data displayed in this work are obtained using a standard telecom DFB MQW DL (by Mitsubishi) giving a few milliwatts tunable single-frequency around 1312 nm. Nonetheless, in several similar setups we employed DFB–DLs of different origin operating at different wavelengths, and we established that the same cavity transmission signals are always observed, with similar timescales and signal to noise levels.

The DL is mounted in a sealed cylindrical housing and is thermoregulated to high precision using a Peltier element and a thermistance. The laser beam is collimated (along the axis of the cylinder) via an aspheric lens with 0.5 numerical aperture, directly mounted on the housing. The laser driving current (repetitive ramps) is supplied by a low noise current source (ILX Lightwave Model LDX3620). A beam splitter permits recording the laser power with an InGaAs photodiode, then the laser beam is reflected by a steering mirror on a PZT actuator before entering the V–cavity. A second photodiode detects the signal at cavity output. Typical photodiode gains are between 10^5 and 10^6 V/W, and a bandpass of 1 MHz is largely sufficient.

The important control parameters for OF locking are the fraction of returning radiation (feedback rate) and its optical phase. The first is controlled by a variable attenuator, obtained here with a polarizer since the DL emission is 99% linearly polarized. In order to maitain the polarization at the V-cavity input aligned with its polarization modes (split with respect to the vertical/horizontal directions due to non–zero incidence angle on the folding mirror), we rotate the LD rather than the polarizer.

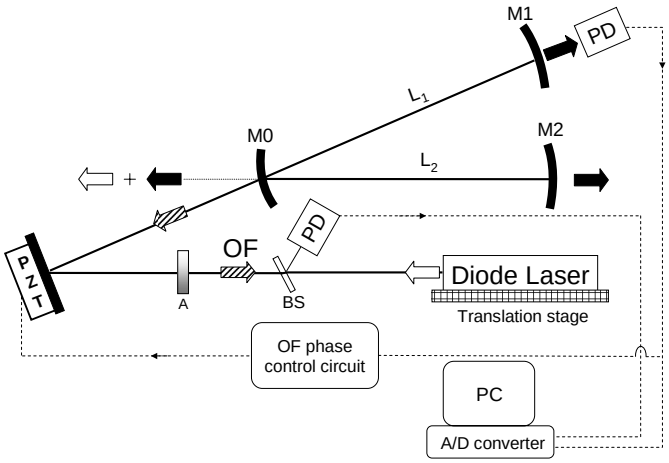

Fig. 1 The V–shaped cavity setup: The direct reflection at the folding mirror does not return to the laser whereas part of the exiting resonant intracavity field gives frequency selective OF. A variable attenuator (A) is used for controlling the feedback rate κ while the PZT-mounted steering mirror adjusts the phase of the OF field. The laser is mounted on a translation stage to allow wider adjustment of the laser–cavity separation. A beam splitter (BS) is used to monitor the power incident on the cavity.

This is easily done thanks to our compact LD cylindrical case. Alternatively, a rotatable half-wave plate could be used for the same task, as well as a second rotatable polarizer. Other attenuation schemes may work as well.

Even if we attenuate the laser beam in both directions, OF cavity injection still gives large signal levels at cavity output, with negligibly low detector and shot noise levels. It is also clear that an adjustable optical isolator could be used to allow injecting all laser power into the cavity, with attenuation occurring only on the returning direction. A signal gain by more than a factor 10 would be obtained, but also increased chances of saturating the molecular transitions. This might occur in applications to trace detection, where transitions are chosen to be as strong as possible and low sample pressure may be needed to improve the separation of absorption lines.

With respect to the OF phase, which depends on the laser–cavity distance, this is finely controlled by subwavelength displacements of the PZT mounted mirror. In a laboratory setup, with a vibrationally isolated optical bench, it is enough to adjust the position of this mirror manually to obtain the correct OF phase for several seconds, enough to acquire several spectra. For automatic operation, we use a simple analogic feedback circuit which exploits the symmetry of the cavity modes as seen in transmission during a frequency scan [34], to produce a real–time error signal for PZT adjustment. We will see that the shape of the cavity modes appear strongly modified due to laser frequency locking by OF. When the OF phase is optimal, the modes assume a rounded symmetric shape, while they are visibly asymmetric in opposite directions when the phase is above or below the optimal point.

We will also see that it is necessary to adjust the laser–cavity distance to be close (to better than 0.5 mm) to the length L_2 of the V–shaped Cavity. This requires using an optical delay line or, as here, mounting the DL on a translation stage.

Another important parameter, simply controlled through the LD injection current ramp, is the tuning speed. This should be sufficiently slow for the OF interaction to take place reproducibly as the laser passes through resonance with each cavity mode. The limit depends mostly on cavity response time. For the high finesse cavities we tested (>10 000), a conservative tuning speed setting corresponds to 0.5 ms per cavity mode.

A sealed glass cell including the cavity mirrors enables using either low pressure samples or a controlled sample flow. An open cavity configuration may be used for direct measurements in ambient air, as reported below. As we work in the near IR, a visible tracing beam (from a HeNe laser or a red DL) is needed for a first laser and cavity alignment. This is injected along one of the cavity arms, through one of the output mirrors. After an IR cavity transmission signal is detected, this is monitored directly to optimize the alignment.

A 12 bits digitizer card in a PC records at a 200 kHz rate the cavity incident power and transmission signals during each laser scan. A higher sampling rate ($\geq$500 kHz) is however needed to register, from time to time, the fast ringdown cavity decay. This is easily produced by shorting out the laser current when this is locked to the top of a given cavity mode, during a scan. A timer card is used to select via software the exact time when this should occur, to allow sampling the ringdown of a predetermined mode in the scan.

The acquisition software written in C language enables efficient real time data processing, including ratioing the two signals, finding the transmission maxima for all modes in the scan, and transforming the cavity transmission to absolute absorbance units. This conversion is possible using the ringdown time. A Voigt lineshape fit is then used to extract sample concentration at a rate up to 10 Hz. For spectra containing more than 2 or 3 absorption lines, lineshape fitting is postponed and streaming the data to a file is preferred.

2 Theory: Diode laser locking to a cavity by resonant optical feedback.

In this section we describe, starting from a theoretical model, the effects induced on laser frequency and linewidth by selective OF from cavity resonances. This

description is fundamental for a physical understanding of how OF can be put to work to deliver efficient and reproducible cavity injection for CEAS measurements.

In the figures of this theoretical section, we also display experimental signals as a support to our discussion of the model. These signals, obtained with the experimental setup discussed above and in conditions of low feedback rates, should be taken as typical of any V-cavity + DFB–DL setup, and show the effect of the parameters mentioned above on the cavity transmission as the laser tunes across several resonances. Comparison with results from the theoretical model will be partly qualitative, given that its adiabatic character does not permit an exact simulation of the dynamical behavior of the laser–cavity coupled system. Still, a fairly good agreement with the observations is obtained. At the end of this section, we will present a plot of experimental data for the cavity injection efficiency as a function of the free–running tuning speed, for different feedback rates. This figure will resume the performance gain afforded by OF, and will be discussed and understood in terms of the theory of laser diode 'self–locking'.

2.1 Diode laser phase noise and linewidth.

DL radiation suffers from a relatively short ($\sim\mu$s) coherence time. In the frequency domain, this corresponds to an average frequency dispersion (the laser spectrum) with FWHM between one MHz for a Multi–Quantum Well DL (MQW–DL) and tens of MHz for HeteroStructure DLs (HS-DL). Indeed, the high cavity losses of these lasers are compensated by high gain levels, which result in high spontaneous emission rates. Spontaneous emission randomly alters the phase of the laser field which builds up from stimulated emission, and poses a fundamental limit to the laser linewidth, as described by the Shawlow–Townes (S–T) equation [40]. It should not come as a surprise that DLs fall very close to this limit, since spontaneous emission easily dominates over technical linewidth broadening effects (e.g. injection current noise). However, this limit has to be slightly redefined, because of the non zero value of Henry's factor α for semiconductor lasers [41, 42], also known as the phase–amplitude coefficient, relating changes in the laser field amplitude to changes in its phase. Physically, this non zero value originates from the dependence of the optical index of the active medium on the population inversion density. Thus spontaneous emission, besides directly inducing a decoherence of the laser field, creates fluctuations in the inversion density which in turn induce phase fluctuations. This enhances the fundamental S–T limit by $1 + \alpha^2$. Henry's factor has values close to 1 for MQW–DLs and ranging roughly from 3 to 8 for HS-DLs depending on the nature of the semiconductor [43].

2.2 Laser linewidth narrowing and frequency locking by optical feedback.

The lack of coherence of DLs is a limiting factor in the efficient injection of high finesse optical cavities [19]. But the coherence may be increased when the frequency–selected optical field originating from a mode of a high finesse cavity is re–injected into a DL. A linewidth narrowing effect is obtained, which can be qualitatively analyzed with a loop scheme involving the cavity ability of converting frequency to amplitude fluctuations. Laser radiation with stable amplitude (relative intensity noise of DLs is extremely low) but high frequency dispersion, is injected into the cavity. Transmitted light possesses a very low frequency dispersion, given by the cavity mode width, but a high level of amplitude fluctuations. When returning part of this radiation into the laser, the saturated gain dynamics dampens those fluctuations (DLs relaxation oscillations occur in the ns time scale). In addition, OF acts as injection seeding at the cavity resonance frequency. Since a DL is a good, low–coherence, broad–band amplifier (on the frequency scale of a cavity resonance), injection seeding is very effective in driving the laser field higly monochromatic. Light finally emitted from the laser–cavity loop has a stable amplitude with a long coherence time. With a cavity finesse of several hundreds and good OF parametrization, the resulting coherence time can be orders of magnitude longer than the cavity response time [30]. Linewidth narrowing, which occurs in a large interval of the OF field phase, will justify considering the laser as a perfect monochromatic source with negligible phase noise, and will account for the smooth 'noiseless' signals observed at cavity output.

In addition to the laser line narrowing effect, OF has a strong effect on the laser emission wavelength, which results in a frequency locking effect. The following simple physical picture may help understanding this effect. Under normal conditions where a positive current ramp is applied to the DL electrodes, the laser tunes to longer wavelengths primarily because the current–induced heating of the active laser region increases the refraction index and thus the laser cavity length. However, when coupling to the external cavity occurs at resonances, one should consider the laser cavity as including the external cavity. The cavity length is then extended to include a high finesse section of effective length up to several km, where a fraction of the laser light circulates. With respect to the rate of laser frequency tuning, the current–induced heating occurs now on a small fraction of the extended cavity, whose resonance condition in much less affected than it is for the free–running monolithic laser cavity. This important slow–down of the frequency tuning rate is in practice equivalent to a frequency locking mechanism.

This physical picture may give the impression that we are dealing with a technique of intra–cavity laser absorption spectroscopy (ICLAS). First of all, ICLAS

is normally used with frequency–multiplexed detection (spectrograph plus linear detector array). From a more fundamental point of view the coupling level to the high finesse cavity containing the sample is rather weak, while in ICLAS the sample is contained in a normal Brewster-windows cell fully included inside the laser cavity. Finally, we measure light power levels in and out of the cavity and obtain the cavity transmission from their ratio thus directly eliminating effects associated with the laser source locking dynamics. The OF-CES technique benefits of this dynamics to achieve an efficient cavity injection and eliminate amplitude noise due to laser phase fluctuations, but its signal ratioing scheme removes a dependence on the details of this dynamics.

2.3 Optical feedback model for a V-shaped cavity.

A simple experimental configuration giving OF from the resonant cavity field is based on injection at the folding mirror of a V-shaped cavity (see Fig.1). In such a configuration, the direct reflection at the input mirror M0 does not return into the laser. Such an OF from a direct reflection would strongly perturb the laser spectrum. When the laser frequency comes to match a resonance, the field which builds–up inside the cavity generates four exiting beams, one of which returns towards the laser. A fraction of its intensity, P_{OF}, will actually inject the laser, after accounting for the attenuator and the spatial coupling factor of the cavity mode (TEM_{00}) with the laser mode. We come therefore to the definition of the OF rate $\kappa = P_{OF}/P_{Laser}$ (where P_{Laser} is the laser intensity).

The OF phase is also a crucial parameter, as it must be inside a range of values (whose extent increases with the feedback rate) to allow efficient frequency locking at a passage through resonance. With respect to cavity injection, most relevant is the effect of the OF phase upon the laser frequency behavior (frequency locking). On the other hand, strong linewidth narrowing may be assumed to be in place as soon as the OF phase combined with the OF rate allow frequency locking. Thus, linewidth narrowing has a fixed effect as it always assures an efficient injection as if a monochromatic field was produced. As it will become clear, the main point is that, depending on the phase, feedback locking occurs to some frequency lying inside the transmission profile of a cavity resonance but not necessarily the center frequency. Then, even if the laser may be considered monochromatic, cavity transmission will not always achieve the value corresponding to the peak of the resonance profile.

We now adapt to our V-cavity configuration the derivation given previously for a confocal cavity [30]. The problem can be analyzed by considering stationary solutions of the coupled system. Writing the lasing condition (conservation of the laser field after one round trip of the free laser cavity where the output facet of the DL is replaced by an effective reflectivity function taking into account the spectral response of the coupled cavity) leads to an expression for the frequency ($\omega = 2\pi c/\lambda$) of the coupled system. In case of weak feedback, the coupled laser frequency ω is implicitly given by [30]:

$$\omega_{free} = \omega + \frac{\sqrt{\kappa(1+\alpha^2)}}{2\pi\tau_{DL}} \times \left[P(\omega)\sin(\omega\tau_0+\theta) - Q(\omega)\cos(\omega\tau_0+\theta)\right] \quad (1)$$

where ω_{free} is the free running laser frequency (directly driven by the laser injection current), τ_{DL} is the free DL photon lifetime, $\tau_0 = 2L_0/c$ is the round trip time, where L_0 is the distance from the output laser facet to the mirror M0, and $\theta = \arctan(\alpha)$. $P(\omega)$ and $Q(\omega)$ are the real and imaginary part, respectively, of the OF field transfer function given for a V-cavity by:

$$F(\omega) = \frac{\mathcal{T}\sqrt{\mathcal{R}}\exp\left(-2\,i\frac{\omega}{c}L_1\right)}{1-\mathcal{R}^2\exp\left[-2\,i\frac{\omega}{c}(L_1+L_2)\right]} \quad (2)$$

where $\mathcal{T}$ and $\mathcal{R}$ are cavity mirror transmission and reflection coefficients respectively (assuming identical mirrors). L_1 and L_2 are defined in Fig 1. For high finesse cavities, Eq.1 can be rewritten as:

$$\omega_{free} = \omega + \sqrt{\kappa(1+\alpha^2)}\frac{c}{2n_0 l_{DL}}\frac{\mathcal{F}_{cav}}{2\mathcal{F}_{DL}} \times \frac{\sin\left[\frac{2\omega}{c}(L_0+L_1)+\theta\right] - \mathcal{R}^2\sin\left[\frac{2\omega}{c}(L_0-L_2)+\theta\right]}{1+(2\mathcal{F}_{cav}/\pi)^2\sin^2\left[\frac{\omega}{c}(L_1+L_2)\right]} \quad (3)$$

where n_0 and l_{DL} are the optical index (in the absence of carriers) and the length of the DL cavity respectively. $\mathcal{F}_{DL}$ is the DL cavity finesse equal to $\pi\sqrt{\mathcal{R}_{DL}}/(1-\mathcal{R}_{DL})$ where $\mathcal{R}_{DL}$ is the laser facet reflectivity. $\mathcal{F}_{cav} = \pi\mathcal{R}/(1-\mathcal{R}^2)$ is the V–cavity finesse with $\mathcal{R}$ approaching unity. The last term of Eq.3 comes from the cavity resonance back–reflection profile of Eq.2. Depending on the cavity mode frequency and the L_0, L_1 and L_2 distances, the coupled laser frequency displays a behavior which is determinant to cavity injection efficiency.

Let us illustrate one specific case. By adjusting L_0, we can make the second term in Eq.3 to vanish at a given resonance $\omega = \omega_n = n\pi c/(L_1+L_2)$ (where n is an integer), so that the coupled laser frequency equals the free running frequency. For $\omega = \omega_n$ it is easy to see that the two sines in the numerator of this term both vanish for $L_0 = L_2 + (L_1+L_2)(m/n - \theta/2\pi n)$ (m is another integer). From inspection of the argument of the first sine in Eq.3 we see that this is equivalent to ask the re–injected field phase to be $-\theta$. This phase is $\phi_n = 2(L_0+L_1)\omega_n/c$, as obtained by considering the field propagating from the laser up to mirror M1 and back. In Fig.2, we plot the coupled laser frequency as a function of the free laser frequency around a resonance, for the above conditions. Since sine terms are zero at resonance, linearizing Eq.3 gives a simple expression, which reveals the dispersive part of the resonance and also gives a good approximation to the plot of Fig.2. The two curves in this plot, obtained for different OF rates, show regions of the free

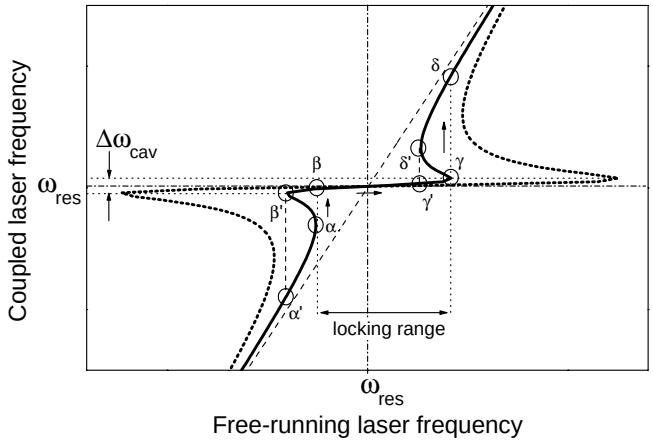

Fig. 2 Detail of the coupled–frequency behavior around a cavity resonance induced by the π–phase shift of the resonant OF, calculated for two OF rates (solid and dotted lines), gives rise to a locking interval. The laser–cavity round trip phase is fixed here to $-\theta$ (see text). The physical behavior of the coupled frequency when monotonically tuning $\omega_{\rm free}$ upward, is obtained by following α-β-γ-δ. When tuning up and down, hysteresis loops are obtained by following α-β-β'-α', or γ-δ-δ'-γ'. The dashed straight line has unity slope and corresponds to the case with no OF and fixes the horizontal scale with respect to the vertical scale.

frequency where three solutions for the coupled laser frequency coexist. When ω_{free} scans up or down, the coupled frequency ω can never enter the negative slope regions, and frequency jumps must occur. These jumps correspond to hysteresis loops, as explained in the caption of Fig.2.

Therefore, close to a cavity resonance, despite a current variation corresponding to an important change in the free running laser frequency, the coupled laser only tunes over a small spectral region falling inside the resonance profile. We will see that this "frequency–locked" interval shifts around depending on the OF phase. The width of the free–running frequency interval over which the laser stays locked to the resonance is defined as the "locking range" [30]. Eq.3 indicates that the locking range increases as the square root of the OF rate (and as the ratio of cavity and laser finesses). As the laser scans through a resonance, the transmitted intensity profile will then appear as a "zoom" (on the horizontal frequency scale) of just a section of the cavity transmission profile, with a zooming factor increasing with the OF rate.

2.4 Mode by mode tuning using optical feedback locking.

When tuning the laser over successive cavity modes, the wavelength change affects the number of oscillations of the laser field on its way to and from the cavity, giving different OF phases. This shifts the locking interval over the resonance profile as illustrated in the top panels of Fig.3. As seen in the central and bottom panels (simulation and experiment), the cavity mode transmission is strongly affected by the OF phase, and the maximum mode transmission may vary from almost zero, up to the maximum of the mode transmission function. Calculated transmitted signals in Fig.3 are based on the stationary solutions (adiabatic limit) of the locked laser frequency which vary as displayed in the top figure panels. The good match with the observed signals, and especially the low noise level on the data (normally associated to laser phase noise), confirms that the laser linewidth falls well below the cavity mode width, even for non optimal OF phase values.

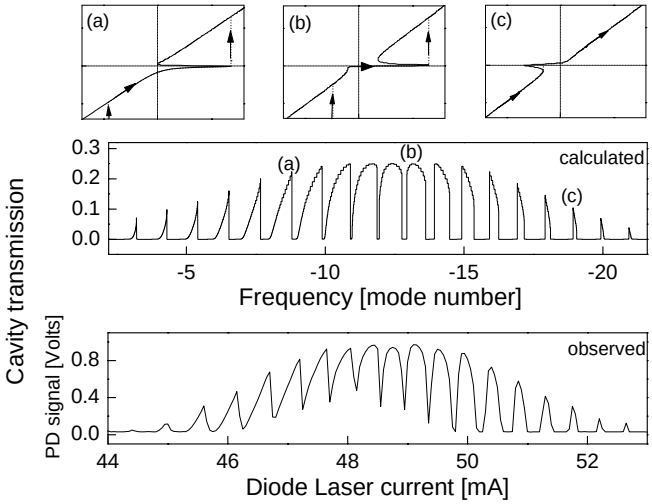

Fig. 3 Comparison of 'typical' calculated (central panel) and experimental (bottom) cavity transmission patterns in the presence of OF. In the top panel are plots of the coupled frequency as a function of free running laser frequency (analogous to that in Fig. 2), calculated for the same OF phase values as for cavity modes 5, 12 and 19 in the central and bottom panels.

In Fig.4, we show a few recorded cavity transmission patterns for different laser–cavity distances. In general, when tuning over several resonances, cavity transmission will reveal a beating pattern. The beating period can be found by imposing that the OF phase change considered before be a multiple of 2π: $\phi_m - \phi_n = 2\pi k$. This gives $L_0 = (k/N) \times (L_1 + L_2) - L_1$ from the first sine term in Eq.3, or equivalently (for a different value of k) $L_0 = (k/N) \times (L_1 + L_2) + L_2$ from the second term, where $N = m - n$ is the period expressed in term of cavity FSRs. In order to have the same OF phase for all modes, we may choose an infinite period (or equivalently a period 1), corresponding to L_0 equal to L_2 plus any multiple of $L_1 + L_2$.

Recorded transmission patterns in Fig.3 and Fig.4 are obtained with an OF rate just below 10^{-4}. Fig.5

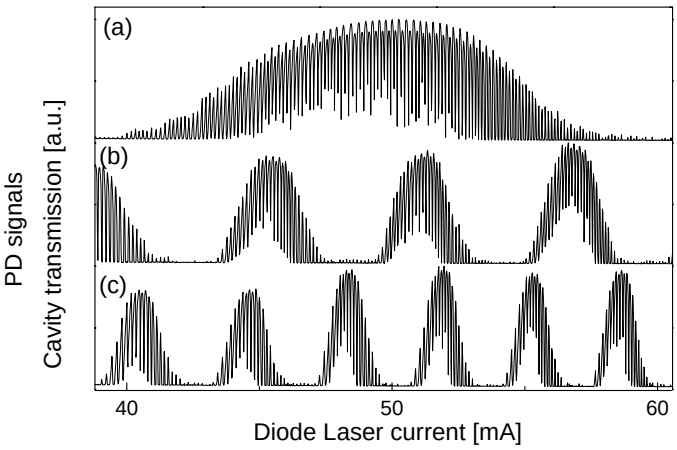

Fig. 4 Cavity transmission patterns for different laser–cavity distances. When approaching the condition $L_0 = L_2$ (from c to a), the beating period increases, and becomes infinite when all modes have the same OF phase.

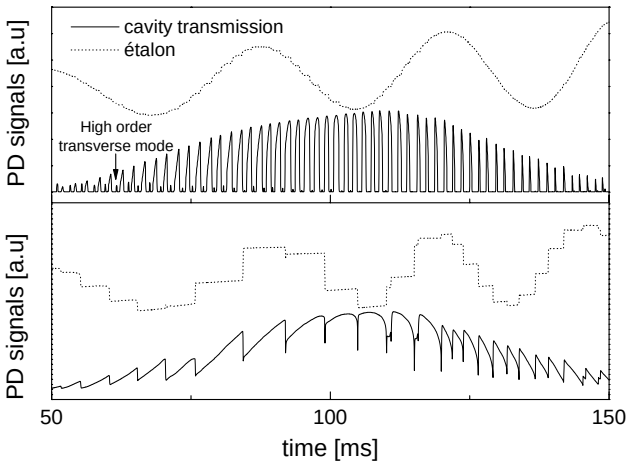

Fig. 5 Cavity transmission patterns for two OF rates. Top panel $\kappa \sim 2\times10^{-5}$. Bottom panel $\kappa \sim 7\times10^{-4}$. The etalon signal (FSR=3.45GHz) monitors the laser frequency behavior: Flat regions are when the laser frequency is locked. For high OF rates, the laser frequency may jump from one resonance to another (even 2 or 3 FSRs away) without passing through the free–running condition.

shows two transmission patterns with the same laser–cavity distance but with different OF rates. In order to monitor the locked frequency behavior, the signal from a flat and uncoated etalon (FSR=3.45 GHz) is also presented. For the highest OF rate, about 10^{-3}, the locking interval becomes sometimes larger than two cavity mode spacings (FSR=170.45 MHz, $L_1 = L_2 = 44$ cm) causing missed cavity modes in a laser scan. It is also interesting to note that the locked laser frequency jumps from one resonance to another without passing through the free running condition, as revealed by the etalon signal.

2.5 Injection efficiency versus tuning speed and feedback level.

All previous discussions of static OF parameters (phase and amplitude) are based on stationary solutions of the coupled system and are justified for values of the free–running frequency tuning speed W below a limit given by the narrowest bandpass in the system, the cavity mode width $\Delta\nu_{cav}$, over the slowest response time, the ring-down time: $W < \Delta\nu_{cav}/\tau_{\rm cav}$.

Analysis of cavity transmission for higher tuning speed (the main dynamic parameter of the system) should account for faster time scales. DL dynamics is governed by combined response times of the medium ($\sim 10^{-13}$ s for semiconductors), photons and carriers (lifetimes of $\sim 10^{-12}$ s and $\sim 10^{-9}$ s, respectively). These are more than three orders of magnitude below the high finesse cavity response time. While it is hard to treat the mathematical model in the fast tuning regime and gain direct insight into the problem, it seems clear that the transient dynamics of the coupled system (before linewidth narrowing) is dominated by the initial cavity build–up. As soon as the laser frequency reaches a cavity resonance, the intracavity field grows linearly with time, at a rate proportional to the laser power. After a few round trips inside the cavity (and from cavity to laser), the field build–up is reinforced by linewidth narrowing, which continues to well below the cavity mode width. This explains why smooth transmission profiles very similar to those given by the adiabatic model for $W < \Delta\nu_{cav}/\tau_{\rm cav}$ are observed in practice even for high tuning speeds. This qualitative picture leads to the simple model below which accounts for the dependence upon κ of the threshold tuning rate above which OF locking breaks down.

Fig.6 shows cavity injection efficiency profiles as a function of the free–running tuning speed for increasing OF rates. These are obtained with the setup described above by recording the maximum of the cavity intensity transmission when tuning the laser through a resonance with optimized feedback phase. In addition, in order to measure the OF rate, a third photodiode records the power returning from the cavity and sampled by the beamsplitter. To set different κ values, we use neutral density filters in place of the polarizer, to insure that polarization to and from the laser is the same and to allow sampling the same fraction of the laser beam in both directions. However, since the coupling factor of the excited $\rm TEM_{00}$ cavity mode with the laser mode is not easily accessible, the reported values of κ are still upper limit estimates. For the same reason, the measured transmission should underestimate the real injection efficiency, but we scale all the transmission profiles so they go to 1 in the limit of slow tuning. The same would

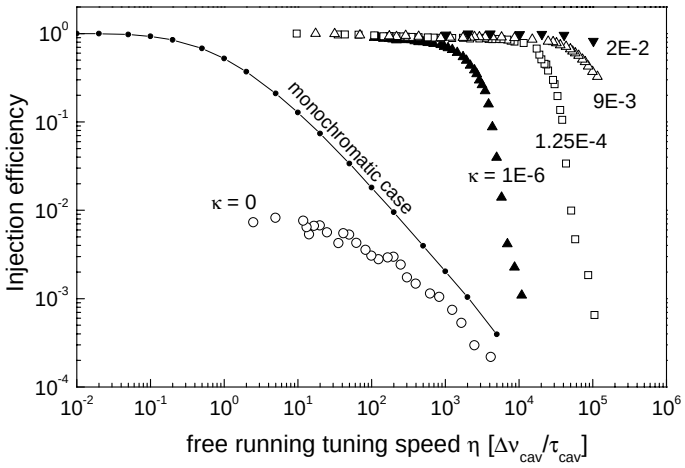

Fig. 6 Cavity injection efficiency as a function of the tuning speed. The scatter–line plot corresponds to a perfectly monochromatic wave. The curve below it corresponds to the no–feedback case. Curves above it are for increasing OF rates. Injection efficiency with OF can be more than two orders of magnitude larger at tuning speeds three orders of magnitude faster.

be obtained by dividing out the maximum H_{max} of the theoretical cavity transmission function, given by Eq.5 below. This eliminates one parameter from the plot, that is, cavity losses (e.g. mirrors coating absorption and scattering). The plotted profiles would apply to the ideal case where light may leave the cavity only by mirror transmission. For any real situation it is then possible to estimate the scaling factor H_{max} and apply it to the injection curve of interest. In addition, the frequency tuning speed is expressed in units of $\Delta\nu_{cav}/\tau_{\rm cav}$. Again, given a real case, the cavity linewidth and the corresponding ring-down time (one is the reciprocal of the other!) are used to determine the position on the horizontal scale. This choice of reduced adimensional units makes the plotted curves "universal". For comparison, in the same figure we also present the injection curves without feedback ($\kappa = 0$) and for an ideal monochromatic laser [19].

When we tune across the cavity mode width in a time equal to the cavity response time, the intracavity buildup starts to become frustrated. This accounts for the monochromatic injection falling down for tuning speeds larger than 1. For $\kappa = 0$ injection starts lower by a factor given by the ratio of the laser to the cavity linewidth. Physically, this corresponds to the fraction of laser power fitting in the cavity mode bandpass [19]. When the tuning speed is such that the laser coherence time becomes equal to the time of passage through a cavity mode, then the $\kappa = 0$ curve joins the curve for the monochromatic case.

2.6 A simple model for the breakdown of feedback locking at high tuning speed.

In the presence of OF, injection starts as high as for a monochromatic wave, due to laser linewidth narrowing. This transmission level is maintained for tuning speeds faster then 1 thanks to frequency locking which increases the time during which the laser stays on resonance and allows for complete cavity buildup. Finally, when the tuning speed is increased beyond a certain limit, which grows with the OF rate, intracavity buildup does not have time to occur and produce significant OF values. This gives a sudden breakdown and a rapid fall of the injection with the tuning speed. In practice, one observes that the transmission pattern becomes weaker but also unstable, with peaks that occasionally totally disappear when looking at successive laser scans. In this breakdown regime, the fast falling edges in Fig.6 are experimentally obtained as average injection values. The appearence of instability should be a signature of the laser phase noise before linewidth narrowing occurs. However, the tuning speeds for which the breakdown occurs are already quite large (even for the $\kappa = 10^{-6}$ case of Fig.6) and the time needed for the laser spectrum to pass through resonance is quite close to the Fourier limit for its free running linewidth. This implies that the laser spectrum may already be considered, to the effect of cavity injection, as a monochromatic wave [19].

In this limit, a simple model accounts for the breakdown tuning speed as a function of the feedback rate κ. The time of passage through resonance, in the monochromatic limit, is given by the cavity mode width over the tuning speed, $\tau_p = \Delta\nu_{cav}/(W\Delta\nu_{cav}/\tau_{cav}) = \tau_{cav}/W$ (where we account for the units of W defined above). The initial linear intracavity field build–up at resonance gives a backward field from the cavity $E_{OF}(t) = E_0\mathcal{T}t/t_r$, where E_0 is the field at the cavity input, and $t_r = 2(L_1 + L_2)/c$ is the cavity round–trip time. We are then interested to know if the buildup occurring during the passage through resonance will achieve a minimum (intensity) feedback level κ_0 needed for OF locking, thus $\sqrt{\kappa_0}$ for the field. In calculating the field level coming back to the laser we have to consider that the steady–state feedback rate κ, being defined as the fraction of laser power reinjected as feedback, accounts not only for the attenuator, but also for the cavity losses and the mode matching factor. Cavity losses are accounted in the factor H_{max} given below in Eq.5, and we will assume 100% mode matching, so that κ/H_{max} is the light intensity attenuation going from laser to cavity and back. The demand posed above is then written as $\sqrt{\kappa/H_{max}}\mathcal{T}\tau_p/t_r > \sqrt{\kappa_0}$, giving the limiting tuning speed $W_{max}(\kappa) = \mathcal{T}(\mathcal{F}_{cav}/2\pi)\sqrt{\kappa/\kappa_0 H_{max}}$. This expression fits the position of the falling injection corners in Fig.6 when the only adjustable parameter κ_0 assumes a value of about 10^{-7}. This value is physically consistent

with the common observation that a DL is sensitive to OF intensity rates as low as 10^{-7}.

We conclude that OF enables injection efficiency orders of magnitude better than without feedback. In the presented case, a gain of 2 orders of magnitude is related to the laser linewidth being 100 times larger than the cavity modes. Even more important, this efficiency is maintained for tuning speeds orders of magnitude faster than for the monochromatic case, which has a large impact on the data acquisition rate. It is also remarkable that with DFB–DLs we never observed chaotic behavior even for OF rates as high as 2×10^{-2}. This is not the case in similar experiments using normal "Fabry-Perot" DLs, which manifest mode hops already with small feedback levels. In these devices, single mode operation is never complete: A parasitic longitudinal laser mode may come to resonance with a cavity mode and pick up feedback at a different time than the principal mode. This mode may then grow up and lock, which corresponds to a laser mode hop.

3 Applications to absorption spectroscopy and trace detection

In this section we first discuss how the OF level and its phase are to be set and optimized to allow observing reproducible high quality CEAS spectra. In particular it is necessary that the OF phase is optimal for all modes during a scan, or, for a sub-ensemble of these, e.g. the "odd" or the "even" modes. We will then explain how absolute absorption coefficients can be obtained when the cavity finesse is known. Several remarks will follow about performance issues, which come to complete the experimental description of the technique. Finally, two simple examples in absorption spectroscopy and trace detection will be presented.

3.1 Optimizing the feedback phase for all modes in a laser scan.

In order to record the peak transmission of successive TEM_{00} cavity modes during a single laser scan, the laser–cavity distance should be adjusted to obtain the same OF phase for all modes. As seen before, this occurs when the optical path DL-M1 is a multiple of the cavity length $(L_1 + L_2)$, which, for the first multiple, is equivalent to setting $L_0 = L_2$. The positioning tolerance depends on the number of excited modes over the tuning range. For example, from the model we find that a beating period of 2000 modes yields a OF phase sufficiently uniform over 200 modes to allow obtaining their transmission maxima in a single scan (during which L_0 is kept fixed). The L_0 positioning tolerance is thus given by $\delta L_0 = \pm(k/2000)(L_1 + L_2)$ which is equal to 0.5 mm for $k = 1$ (first multiple) and $L_1 + L_2 = 100$ cm. After adjusting L_0 to the right value within this tolerance, it is still necessary to act on the PZT–mounted mirror to finely adjust this path at the sub–wavelength scale, in order to drive the OF phase to a value corresponding to maximum cavity injection. After this, the OF rate is adjusted to obtain a locking range slightly smaller than the mode spacing. As explained above, this enables "zooming–in" around the tops of the transmission profile of the resonances as the laser is tuned. The peak transmission of these modes may then be determined by a numerical analysis of the digitized photodiode signals for the cavity input and output.

3.2 Effect of cavity symmetry: Odd and even modes.

Interesting effects are associated with the V-cavity symmetrical geometry, which need to be understood and controlled for optimal CEAS measurements. The stationary waves corresponding to the cavity modes must have nodes on the cavity mirrors M1 and M2. Thus, modes with odd and even number of field oscillations do not have the same phase on the folding mirror M0 and do not suffer the same losses upon reflection, as clearly observed on the transmission patterns of Fig.4. This effect can be corrected at the signal processing stage, or eliminated by choosing a laser–cavity distance giving a favorable OF phase condition for only one family of modes at a time, which is done by increasing the laser–cavity distance by L_2. This "all even" or "all odd" injection scheme allows using a larger κ in order to spread the locking range over two cavity FSRs. In turn, this permits using a higher tuning speed to maintain approximately the same acquisition time per observed mode (one data point in the spectrum). In different setups we tested (different DFB–DLs, but similar cavity finesse) we always achieve a reliable performance with 0.5 ms per mode. The maximum working tuning speed should be set to a value corresponding to the limit of the flat part of the injection curve for a given κ value (Fig.6). In practice, we observe in real time the mode–by–mode CEAS spectrum of an absorption line, then increase the tuning speed until finding the point where the absorption line profile starts appearing perturbed (in noise level and shape).

A disadvantage of injecting only the even or the odd cavity modes is the loss of spectral resolution. For a cavity 100 cm long, the TEM_{00} mode density is just enough to allow proper tracing of absorption line profiles at the Doppler limit (low pressure samples, below 100 mbar). When the effective spacing is doubled, the OF-CEAS spectrometer should be used at higher pressures, as in the examples shown below.

Another fine effect associated with the even–odd cavity modes, is the existence, for each family of modes, of a sinusoidal baseline modulation if $L_1 \neq L_2$. This is again due to the different phase of odd–even cavity standing waves at the folding mirror M0. Looking into more detail, one finds that the folded field on M0

forms a sinusoidal pattern with nodal lines perpendicular to the cavity plane and spatial frequency given by the projection of the wave vector on the mirror plane. The patterns for neighboring odd and even modes are in quadrature ($\pi/2$ out of phase) at each point of the surface: Where one mode has a node, the other will have maximum amplitude. Mirror inhomogeneities will then induce a slight difference in reflection losses between odd and even modes. If $L_1 \neq L_2$ the nodal lines shift as a function of the frequency, and the period for a complete phase cycle is given, in cm^{-1}, by $\Delta\nu_{eo} = 2/|L_1 - L_2|$ (the reciprocal of the displacement of M0 with respect to the cavity center). Over half of this period, the even–odd mode losses undergo an exchange, thus the CEAS spectrum from each family exhibits a sinusoidal baseline modulation (in quadrature for the two families). Due to mechanical and thermal drift of the setup over time, this baseline modulation will slowly shift. However, if the two cavity arms are set equal to better than 1 mm by construction, the beating period will be sufficiently long not to perturb CEAS spectra baseline significantly.

3.3 From cavity transmission to OF-CEAS spectra in absolute absorption units.

In the top panel of Fig.7, we show a cavity transmission signal when all parameters are set as discussed and a current slope from 20 to 80 mA is applied during 100 ms to the DL. Three absorption lines, corresponding to three water vapor transitions around 1312 nm, are visible. The transfer function for intensity transmission of a V–cavity is :

$$H(\omega) = \frac{H_{max}(\alpha(\omega))}{1 + (4\mathcal{F}_{eff}^2/\pi^2)\,\sin^2\left[\frac{\omega}{c}(L_1 + L_2)\right]}\,, \qquad (4)$$

where $\alpha(\omega)$ is the molecular absorption coefficient and $\mathcal{F}_{eff} = \pi\mathcal{R}_{eff}/(1 - \mathcal{R}_{eff}^2)$ with $\mathcal{R}_{eff} = \mathcal{R}\exp[-\alpha(L_1 + L_2)]$. Maxima of the transmitted signal, measured by OF-CEAS, are given by :

$$H_{max}(\alpha_m) = \left[\frac{\mathcal{T}\exp[-\alpha_m L_1/2]}{1 - \mathcal{R}^2\exp[-\alpha_m(L_1 + L_2)]}\right]^2\,, \qquad (5)$$

where α_m is the absorption coefficient taken at the center of the cavity resonance. In the absence of intracavity absorption $H_{max} \simeq [\mathcal{T}/2(1 - \mathcal{R})]^2 = [\mathcal{T}/2(\mathcal{T} + \mathcal{L})]^2$, leading to a maximum cavity transmission of 25% when mirror losses are zero ($\mathcal{L} = 0$).

Quantitative absorption spectra are deduced from peak transmission values of the cavity resonances by applying the inverse function which is easily written if we neglect the term $\exp(-\alpha_m \cdot L_1/2)$ in the numerator of H_{max}. Note that the reflection coefficient of the mirror (or equivalently the finesse or the ringdown time) of the cavity has to be known. Also, as the laser power varies during the frequency sweep, it must be recorded and used for normalization. This also allows to take into account the small variation ($< 1\%$) of laser power which may occurs together with the frequency locking effect. For low absorption levels, we may recover the linear dependence discussed in the introduction. However, the non–linear dependence in Eq.5 for higher absorptions enables a large dynamic range of detection. It is easy to see that the cavity transmission as a function of the absorption coefficient decreases much less rapidly than the Lambert-Beer law $\Delta I/I = \exp(-\alpha L_{eq})$ for the same equivalent path $L_{eq} = (2\mathcal{F}/\pi) \times (L_1 + L_2)$.

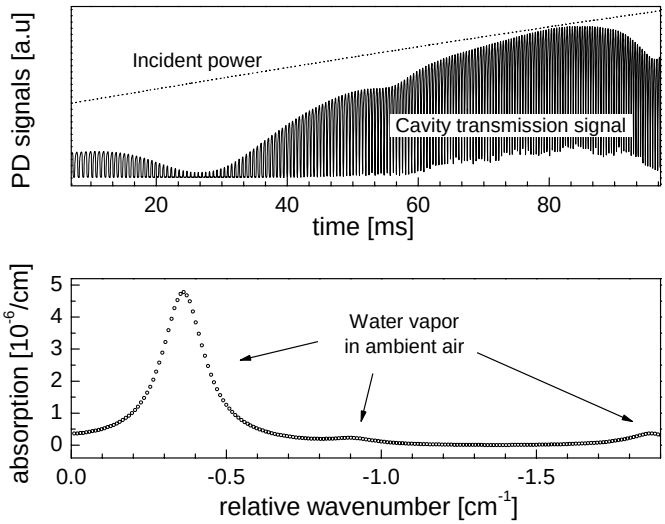

Fig. 7 Top panel: cavity transmission signal with optical feedback parameters optimized for CEAS, together with the incident power signal needed for normalization. By picking the maximum of each 'feedback–enlarged' transmission resonance, a self-frequency calibrated OF-CEAS spectrum is obtained (bottom panel) using Eq.5 and the cavity frequency comb. Three absorption lines of ambient water vapor are visible. The strongest line is at 7618.26 cm^{-1}, assigned by comparison to a spectrum simulated using the HITRAN database. A baseline noise of 2×10^{-9}/cm is deduced from an amplitude shot to shot relative fluctuation of 10^{-3}.

3.4 Performance, spectroscopy, and trace detection.

We give here some complementary technical details about our OF-CEAS setup, especially with respect to performance issues. As already stated, pure TEM_{00} cavity injection is easily obtained even if no special effort is done for transverse mode matching. Indeed, it is enough to have dominant spatial coupling of the laser beam to the TEM_{00} modes to makes their feedback rate much larger than for other transverse modes. In addition, as the locking range to the TEM_{00} modes is set to cover almost a full cavity FSR (by adjusting the attenuator), transverse modes have no chance to ever be excited. For this to work well, it is assumed that the cavity length

is such that no transverse mode is frequency degenerate with the TEM_{00} modes.

As we mentioned earlier, the PZT mirror servo–loop uses the asymmetry of the shape of the cavity transmitted modes as an error signal [34]. The loop band pass should be ultimately limited to about 1 kHz by the tuning time over each cavity mode. The best we obtain in our setup is a band pass of about 100 Hz. This appears to be sufficient even in rather noisy environments, if the setup is vibrationally isolated. Recent tests with two OF-CEAS devices operated onboard an atmospheric research airplane (a NASA DC8 model) [44] demonstrate the robustness of this technique even in a vibrationally hostile environment.

Signals recorded with this system display shot to shot fluctuations on maximum mode transmission $\Delta I/I = 1\times10^{-3}$, corresponding to a noise–equivalent absorption of about 2×10^{-9}/cm for a measured cavity ringdown time around 17 μs. Acquiring 200 modes in 100 ms (Fig.7) gives a point acquisition rate of 2 kHz, and a bandpass–normalized detection limit of $4\times10^{-11}/\mathrm{cm}/\sqrt{\mathrm{Hz}}$. It should be stressed that this figure of merit is not meant to imply that by averaging over e.g. 2000 scans one should achieve a 4×10^{-11}/cm baseline noise level. Indeed, the averaging time after which noise stops decreasing for our setup is met after averaging 10 to 100 scans, leading to a limiting baseline noise of about 2×10^{-10}/cm for 10 s averaging. This is due to the presence of interference fringes induced by reflected and diffused light by optics lying outside the cavity. It is easy to determine in practice which optical element causes most of the trouble as the fringe pattern moves when touching that element (causing its displacement by a fraction of wavelength), it appears however difficult to reduce fringes to below the cited level, even when using high quality optics. This actual limitation, added to the risk of molecular saturation effects at high intracavity fields, justifies our choice of using an attenuator to control the feedback rate instead of a variable isolator. This would allow a higher signal level, but not an improved signal to noise ratio.

Since each data point corresponds in frequency to one or two cavity FSRs, the frequency scale of spectra is linear to a high degree. By recording shot to shot excess intensity fluctuations of a data point situated on the half-height slope of an absorption line profile, we deduce a (shot-to-shot) frequency definition better than 1 MHz on the timescale of a few seconds. In addition, if we calculate the effect of the dispersion induced by an absorption line over the position of cavity modes, we find that their displacement is on the order of only 10 kHz for a Doppler limited line with a 'large' absorption coefficient of 10^{-5}/cm.

To illustrate the high data quality over a large dynamic range, Fig.8 shows a spectrum of ambient air at 1 atm, where two absorption lines are clearly visible. On the left wing of the strongest line is a weak feature, corresponding to a third weak absorption line. All three lines are easily fitted using a conventional Lorentzian multi–peak fitting procedure, without need for fixing any of the line parameters. Such a fit becomes easily unstable for blended lines in the presence of noise level or spectral distortion. A zoom of the left part of the baseline spectrum reveals three other weak absorption lines also nicely fitted by Lorentzian profiles. We thus see that in the same spectrum, acquired in 100 ms, absorption coefficients between 2.2×10^{-8}/cm and 1.3×10^{-5}/cm are measured. This gives to the OF-CEAS technique a great potential for high precision measurements over a large dynamic range.

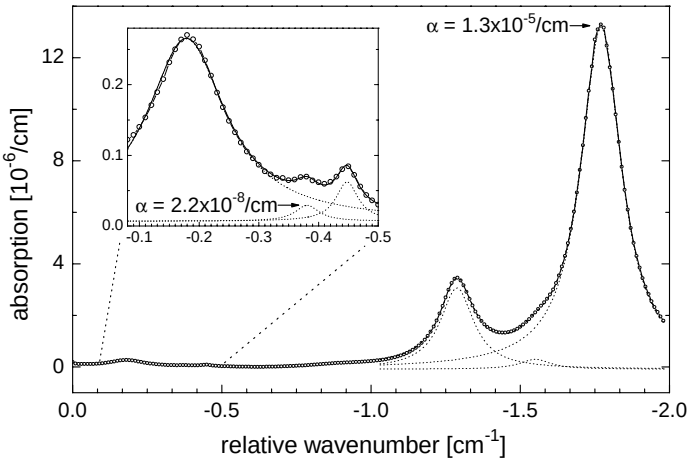

Fig. 8 Water lines in ambient air around 1312.3 nm. Six absorption lines are present on the same spectrum covering three intensity decades. The high data quality over the entire dynamic range enables a precise lineshape fit of all these features. Position of the strongest line is 7620.28 cm^{-1}, deduced by comparison with a HITRAN simulation.

Finally, we demonstrate real–time trace gas concentration monitoring. HF possesses an intense isolated transition of the first overtone band at 1312.232 nm (P(3) line), easily accessible with a commercial telecom DL like the one used here. This line has a cross section $\sigma = 4.7\times10^{-20}\mathrm{cm}^2$ at 300 K [45]. As HF is chemically reactive (e.g. with cell walls), after injecting HF traces in an open V–shape cell (a simple tube placed in the intracavity space, to avoid air currents), we could record a fast concentration decay. Results are shown in Fig.9. In the bottom panel, spectra corresponding to different HF concentrations are shown. On the left side of the HF line, a water vapor line is also present, which is taken into account in the fitting procedure to allow obtaining reliable HF concentrations. In the top panel is a log plot of the concentration over several minutes, which demonstrates a dynamic range close to four orders of magnitude and sub–ppb HF detection. Using a 200 MHz pentium processor, our system was able to fit the absorption lines at a rate of about 10 Hz.

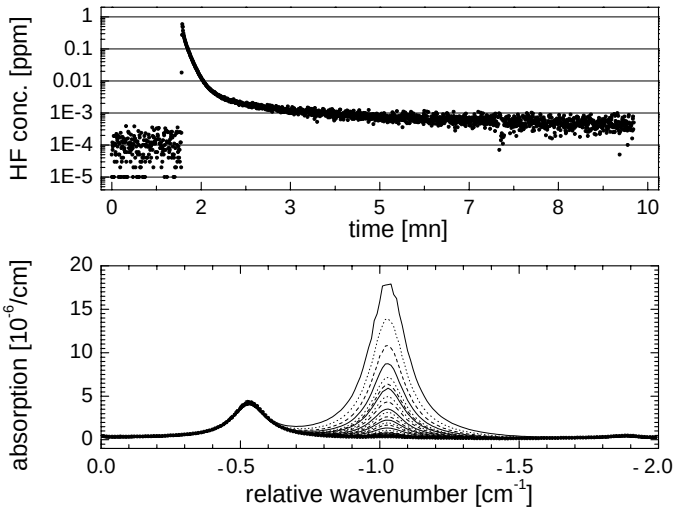

Fig. 9 Real time monitoring of HF at 7618.52 cm^{-1} at the P(3) transition. Response time is 0.1 s. Detection is sub–ppb. Dynamic range spans nearly four orders of magnitude.

4 Conclusions and perspectives

To our knowledge, we presented the first experimental results for optical locking to a cavity with a V geometry. In contrast to previous work based on confocal cavities, this geometry allows OF locking with much higher cavity finesses. We showed that OF enables measurement of the maximum transmission of cavity modes with a signal to noise ratio of at least 10^3, yielding a cavity enhanced spectrum when performed on successive modes covered by a fast laser scan. This appears to give a serious advantage with respect to electronic frequency locking schemes. Since the acquisition rate is a crucial parameter, we studied the cavity injection efficiency as a function of the free–running laser tuning speed. The gain in injection with OF is more than two orders of magnitude even using tuning speeds three orders of magnitude higher, when comparing to the widespread no–locking, no–feedback, CEAS schemes.

We gave details about optimal parameter choice for the coupled cavity–laser system (laser–cavity length, OF rate, tuning speed), and demonstrated the performance of the technique. Given the high signal level at cavity output, and the low intrinsic noise of DL sources, shot–noise limited detection is in principle possible (with up to 100 times lower noise level), but only after getting rid of the parasitic fringes appearing on OF-CEAS spectra. In contrast to other cavity–enhanced schemes, including those based on all–electronic laser frequency locking, OF-CEAS is expected to function reliably with cavities having higher finesse than reported here.

The high data quality, on both vertical and horizontal (frequency) scales is essential for high precision measurements. In fact, data points in the OF-CEAS spectra are taken on the uniform frequency comb of the TEM_{00} cavity modes, which do not move appreciably during the short time of a laser scan. The fast acquisition rate allows real time monitoring of the concentration of a species through detection of one of its absorption lines. As an example, detection of the reactive HF molecule was performed around 1312 nm, with a cell open to ambient air, down to sub-ppb levels. The time resolution was 0.1 s and the concentration dynamic range close to four orders of magnitude. An advantage when using a closed V-cavity configuration, with respect to usual multipass cells, is the small sample volume. This can be easily reduced down to 10 cm^3 for a 50 cm long V-cavity. The spacing of points in a OF-CEAS spectrum (150 MHz) is sufficient to describe the profile of absorption lines at low pressure and allows to derive their Doppler width with excellent accuracy.

The OF-CEAS technique requires only a few optical components and is well adapted to the realization of compact, low consumption, and affordable trace gas detectors. Recent successful tests onboard a NASA DC8 airplane demonstrate its robustness [44]. Even though results reported here are based on a DFB–DL at 1312 nm, OF-CEAS works well with any DFB–DL diode laser and, according to recent tests, even with grating–tunable diode lasers (ECDLs). Detailed results on the measurement of several atmospheric traces (CH_4, NH_3, CO_2 H_2S..., H_2O and CH_4 isotopologues...) using telecom DFB DLs will be presented in the near future. We also plan to test the method with quantum cascade lasers for accessing stronger fundamental molecular transitions in the mid-infrared spectrum.

5 acknowledgments

We would like to thank M. Prevedelli (University of Bologna) for his help in this development. Financial support by the Bureau of Industrial Relations of the University J. Fourier of Grenoble is gratefully acknowledged.

References

1. A. Kastler, Applied Optics **1**, 17 (1962).
2. D. Z. Anderson, J. C. Frisch, and C. S. Masser, Applied Optics **23**, 1238 (1984).
3. A. O'Keefe and D. A. G. Deacon, Review of Scientific Instrument **59**, 2544 (1988).
4. D. Romanini and K. K. Lehmann, Journal of Chemical Physics **99**, 6287 (1993).
5. D. Romanini, A. A. Kachanov, N. Sadeghi and F. Stoeckel, Chemical Physics Letters **264**, 316 (1997).
6. G. Berden, R. Peeters and G. Meijer, International Reviews in Physical Chemistry **19**, 565 (2000).
7. B. A. Paldus, C. C. Harb, T. G. Spence, B. Wilke, J. Xie, J. S. Harris and R. N. Zare, Journal of Applied Physics **83**, 3991 (1998).
8. T. G. Spence, C. C. Harb, B. A. Paldus, R. N. Zare, B. Willke and R. L. Byer Review of Scientific Instruments **71**, 347 (2000).

9. Y. He and B. J. Orr, Chemical Physic Letter **335**, 215 (2001).
10. J. Ye, L. Ma and J. Hall, SPIE proceedings series **3270**, 85 (1998).
11. L. Gianfrani, R. W. Fox and L. Hollberg, J. Opt. Soc. Am. B **16**,2247 (1999).
12. Nicola J. van Leeuwen and Andrew C. Wilson, J. Opt. Soc. Am. B **21**,1713 (2004).
13. J. Morville, D. Romanini, A. Kachanov and M.Chenevier, Applied Physics B **78** (2004).
14. J. T. Hodges, H. Layer, W. Miller and G. Scace, Review of Scientific Instrument **75**, 849 (2004).
15. N. van Leeuwen, J. Diettrich and A. Wilson, Applied Optics **42**, 3670 (2003).
16. J. Morville, M. Chenevier, A. A. Kachanov and D.Romanini, SPIE proceedings series **4485**, 236 (2001).
17. D. Romanini, A. A. Kachanov and F. Stoeckel, Chemical Physics Letter **270**, 538 (1997).
18. B. Paldus, C. Harb, T. Spence, R. Zare, C. Gmachl, F. Capasso, D. Silvo, J. Baillargeon, A. Hutchinson and A.Cho, Optics Letter **25**, 666 (2000).
19. J. Morville, D. Romanini, M. Chenevier and A.Kachanov, Applied Optics **41**, 6980 (2002).
20. R. W. Drever, J. L. Hall, F. V. Kowalski, J. Hough, G. M. Ford, A. J. Munley and H. Ward, Applied Physics B **31**, 97 (1983).
21. A. O'Keefe, J. J. Scherer and J. B. Paul, Chemical Physics Letter **307**, 343 (1999).
22. R. Peeters, G. Berden, A. Apituley and G. Meijer, Applied Physics B **71**, 231 (2000).
23. D.S. Baer, J.B. Paul, M. Gupta and A. O'Keefe, Applied Physics B **75**, 261 (2002).
24. J. B. Paul, L. Lapson and J. G. Anderson, Applied Optics **40**, 4904 (2001).
25. D. Herriott, H. Kogelnik and R. Kompfner, Applied Optics **3**, 523 (1964).
26. J. Morville, D. Romanini and M. Chenevier, Patent WO03031949, Université J. Fourier, Grenoble (FRANCE) (2003).
27. B. Dahmani, L. Hollberg and R. Drullinger, Optics Letter **12**, 876 (1987).
28. F. Favre and D. Le Guen, IEEE Journal of Quantum Electronics **21**, 1937 (1985).
29. R. F. Kazarinov and C. H. Henry, IEEE Journal of Quantum Electronics **23**, 1401 (1987).
30. P. Laurent, A. Clairon and C. Breant, IEEE Journal of Quantum Electronics **25**, 1131 (1989).
31. H. Li and N. Abraham, Applied Physics Letter **53**, 2257 (1988).
32. H. Li and H. Telle, IEEE Journal of Quantum Electronics **25**, 257 (1989).
33. H. Li and N. Abraham, IEEE Journal of Quantum Electronics **25**, 1782 (1989).
34. S.-I. Ohshima and H. Schnatz, Journal of Applied Physics **71**, 3114 (1992).
35. D. Schnier and A. Madej, Optics Communication **105**, 388 (1994).
36. C. Shin and M. Ohtsu, Optics Letter **15**, 1455 (1990).
37. B. Young, F. Cruz, W. Itano and J. Bergquist, Physical Review Letter **82**, 3799 (1999).
38. C. Tanner, B. Masterson and C. Wieman, Optics Letter **13**, 357 (1988).
39. J. Morville and D. Romanini, Applied Physics B **74**, 495 (2002).
40. A. L. Schawlow and C. H. Townes, Physical Review **112**, 1940 (1958).
41. C. Henry, R. Logan and K. Bertness, Journal of Applied Physics **52**, 4457 (1981).
42. A. Yariv, Quantum Electronics, John Wiley& Sons, New York (1989), 3rd ed.
43. K. Petermann, Laser Diode Modulation and Noise, Kluwer Scientific Publishers, Tokyo (1991).
44. E. Kerstel, R. Iannone, H.-J. Jost, and D. Romanini "A cavity enhanced near–infrared spectrometer for airborne trace–level water isotope (^{2}H, ^{17}O, and ^{18}O) analysis", In preparation.
45. L. Rothman, C. Rinsland, A. Goldman, S. Massie, D. Edwards, J.-M. Flaud, A. Perrin, C. Camy-Peyret, V. Dana, J. Mandin, et al., Journal of Quantum Spectroscopic Radiation Transfer **60**, 665 (1998).